Nanoscale

PAPER

View Article Online
View Journal

Cite this: DOI: 10.1039/c9nr07580a

Effects of oral exposure to titanium dioxide nanoparticles on gut microbiota and gut-associated metabolism *in vivo*†

Zhangjian Chen,[a] Shuo Han,[a] Di Zhou,[a] Shupei Zhou[b] and Guang Jia*[a]

Received 2nd September 2019,
Accepted 19th October 2019

DOI: 10.1039/c9nr07580a

rsc.li/nanoscale

The antibacterial activity of titanium dioxide nanoparticles (TiO_2 NPs) has been extensively documented and applied to food packaging or environmental protection. Ingestion of TiO_2 NPs *via* dietary and environmental exposure may pose potential health risks by interacting with gut microbiota. We conducted an animal experiment to investigate the effects of oral exposure to TiO_2 NPs on gut microbiota and gut-associated metabolism in Sprague-Dawley rats. Rats were administered with TiO_2 NPs (29 ± 9 nm) orally at population-related exposure doses (0, 2, 10, 50 mg kg^{-1}) daily for 30 days. Changes in the gut microbiota and feces metabolomics were analyzed through bioinformatics. TiO_2 NPs caused significant changes of colon morphology in rats, manifested as pathological inflammatory infiltration and mitochondrial abnormalities. 16S rDNA sequencing analysis showed that the structure and composition of gut microbiota in rats were modulated after exposure to TiO_2 NPs. Monitoring data demonstrated that differentially expressed bacterial strains were obtained until exposure for 14 days and 28 days, including increased *L. gasseri*, *Turicibacter*, and *L. NK4A136_group* and decreased *Veillonella*. Fecal metabolomics analysis showed that 25 metabolites and the aminoacyl-tRNA biosynthesis metabolic pathway have changed significantly in exposed rats. The increased metabolites were represented by *N*-acetylhistamine, caprolactam, and glycerophosphocholine, and the decreased metabolites were represented by 4-methyl-5-thiazoleethanol, L-histidine, and L-ornithine. Metabolic disorders of gut microbiota and subsequently produced lipopolysaccharides (LPS) led to oxidative stress and an inflammatory response in the intestine, which was considered to be a key and primary indirect pathway for toxicity induced by oral exposure to the TiO_2 NPs. In conclusion, orally ingested TiO_2 NPs could induce disorders of gut microbiota and gut-associated metabolism *in vivo*. The indirect pathway of oxidative stress and inflammatory response, probably due to dysbiosis of gut microbiota primarily, played an important role in the mechanisms of toxicity induced by oral exposure to TiO_2 NPs. This may be a common mechanism of toxicity caused by oral administration of most nanomaterials, as they usually have potential antimicrobial activity.

1. Introduction

Engineered nanomaterials (ENM) have been widely used in the food industry as food additives or antimicrobials for improving food preservation, *etc.*[1,2] Ingestion of ENM *via* dietary intake can be an important pathway of human exposure to nanoparticles.[3] Titanium dioxide nanoparticles (TiO_2 NPs) are one of the most promising engineered nanomaterials that have widespread application on commercial, industrial, and environmental scales. Titanium dioxide (TiO_2) is a white pigment with great brightness and a very high refractive index, which has been used in an ultrafine form as a white coloring (referred to as food-grade additive E171 in the EU) for confectionery, sauces, cakes, and pastries.[4] Recently, two studies suggested that up to 36% of the food-grade TiO_2 particles are nanoparticles.[5,6] A study also showed that over 40% of TiO_2 particles in commercial gums are TiO_2 NPs, which can leach out and be swallowed when chewing.[7] Indeed, it has been estimated that the human dietary exposure dose of TiO_2 NPs has reached 2.16–100 microgram per kilogram body weight per day (μg per kg bw per d).[6,8] Due to their excellent photocatalytic activity, TiO_2 NPs have also been widely used for self-cleaning surfaces and water/atmosphere purification.[9–11] The inevitable release of TiO_2 NPs increased the predicted environmental concentration up to 0.7–16 μg L^{-1} (Mueller and Nowack, 2008),

[a]*Department of Occupational and Environmental Health Sciences, School of Public Health, Peking University, Beijing 100191, China. E-mail: jiaguangjia@bjmu.edu.cn*
[b]*Department of Laboratory Animal Science, Health Science Center, Peking University, Beijing 100191, China*

†Electronic supplementary information (ESI) available. See DOI: 10.1039/c9nr07580a

which posed a risk for organisms and humans. One of the latest studies detecting TiO_2 particles in human post-mortem liver and spleen showed that more than 24% of TiO_2 particles were NPs and the authors emphasized that health risks due to oral exposure to TiO_2 NPs should be paid sufficient attention.[12]

The fate of TiO_2 NPs after oral administration in the body and their potential health effects have been studied a lot.[13,14] After their ingestion, TiO_2 NPs pass through the digestive tract, where they may undergo interactions with the gut microbiota in the luminal environment, before crossing the epithelial barrier to reach the systemic compartment. Considering that only about 0.02%–0.1% of TiO_2 NPs could be absorbed through the gastrointestinal (GI) tract and the rest were excreted through feces,[15–18] the effects in the GI luminal environment should account for the largest proportion of the systemic toxicity caused by TiO_2 NPs. As an important part of human and animal composition, gut microbiota is increasingly recognized to play crucial roles in the maintenance of host health.[19,20] A number of studies in recent years have demonstrated that dysbiosis of gut microbiome can affect energy metabolism, nutritional digestion and absorption, immune status, inflammatory reaction and the occurrence and progress of many diseases.[21–23] Furthermore, gut microbiota dynamics is highly sensitive to exogenous stressors, environmental pollutants being of particular concern.[24] Therefore, we speculated that TiO_2 NPs by oral administration may interact with gut microbiota, thereby affecting host metabolism and indirectly causing a series of biological effects including extra-intestinal organs.

The antimicrobial activity of nanoparticles, especially metal and metal oxide NPs, has attracted the attention of scientists.[25] Oxidative stress *via* the generation of reactive oxygen species (ROS) on surfaces of the nanoparticles may be one of the mechanisms.[26] Many research studies have proved that the particle size is a significant factor which indicates the antimicrobial effectiveness of NPs.[27] The use of NPs as an antimicrobial component especially in food additives and medical applications can be one of the new and considerable strategies for overcoming pathogenic microorganisms.[28] The antibacterial activity of TiO_2 NPs, facilitated by the generation of ROS, has been extensively documented *in vitro*.[29,30] And the TiO_2 NPs with an anatase crystal structure and a smaller particle size produced a higher content of intracellular ROS and malondialdehyde (MDA), in line with their greater antibacterial effect.[31] Photocatalytic properties of the TiO_2 NPs help them to efficiently eradicate the bacteria.[32,33] Later, Sohm *et al.* found that 10 mg ml^{-1} of TiO_2 NPs could destroy the integrity of the *E. coli* cell membrane under dark conditions, and then cause osmotic stress.[34] In the absence of light, TiO_2 NPs also have the ability to disrupt bacterial cell walls and cause cell death by producing ROS.[34,35] Moreover, in an *in vitro* model colon, TiO_2 NPs were reported to impact gut microbiota and disturb the production of short-chain fatty acids.[36–38] However, there is still a lack of research about the effect of TiO_2 NPs on the gut microbiota *in vivo*.

The present study aimed to explore the effects of oral exposure to TiO_2 NPs on gut microbiota and gut-associated metabolism in Sprague-Dawley rats. Structure and abundance changes of gut microbiota were monitored by 16S rDNA sequencing analysis in stool samples of rats after oral exposure to TiO_2 NPs for 7, 14 and 28 days. Meanwhile, metabolic changes of feces were analyzed through non-targeted metabolomics using HPLC-MS. Host overall fitness and intestinal health were also determined and analyzed alongside the dysbiosis of the gut microbiota. By using bioinformatics methods and detecting several typical metabolites, the effects on gut microbiota induced by oral administration of TiO_2 NPs were studied comprehensively.

2. Methods

2.1 Nanoparticle characterization

Titanium dioxide nanoparticles (TiO_2 NPs) were purchased from Shanghai Macklin Reagent Co. Ltd, China. The size and shape of the particles were characterized by scanning electron microscopy (SEM, Nova, Tecnai F30, FEI Company, Oregon, USA). Energy dispersive X-ray spectroscopy (EDS, Nova_NanoSEM430, FEI Company, Oregon, USA) was used to measure the ratio of Ti to O atoms. The purity of the particles was analyzed by inductively coupled plasma atomic emission spectroscopy (ICP-AES, IRIS Advantag, TJA, Franklin, MA, USA). The crystal structure of the particles was identified by X-ray powder diffractometry (XRD, PANalytical's X'Pert PRO, X'Celerator, EA Almelo, Netherlands). The specific surface area (SSA) of the particles was measured according to the Brunauer–Emmett–Teller (BET) method (Quantachrome, Autosorb 1, Boynton, FL, USA).

Artificial gastric juice (AGJ, pH = 1.2) was prepared using 10 g L^{-1} pepsin (3800 units per mg) and 45 mmol L^{-1} HCl. Artificial intestinal juice (AIJ, pH = 6.8) was made with 10 g L^{-1} trypsin (2500 units per mg) and 6.8 g L^{-1} KH_2PO_4. The pH was adjusted to 6.8 using 0.1 mol L^{-1} NaOH. TiO_2 NPs were dispersed in ultrapure water (H_2O), and AGJ or AIJ to obtain a final concentration of 1 mg mL^{-1}. Then, the suspensions were supersonicated for 15 min to break up aggregates. The particle hydrodynamic diameters and zeta potentials were tested using a ZetaSizer Nano ZS90 (Malvern Instruments Ltd, Malvern, UK).

2.2 Animal and experimental design

Three-week-old healthy Sprague-Dawley rats were bred and supplied by the Department of Laboratory Animal Science, Peking University Health Science Center. The rats were fed a commercial pellet diet and deionized water *ad libitum*, and kept in plastic cages at 20 ± 2 °C and 50–70% relative humidity with a 12 : 12 h light–dark cycle. After one week of acclimation, rats were weighed and randomized into experimental and control groups, with 6 male rats in each treatment group.

All experimental rats were cared for humanely. The study was conducted in accordance with the Guiding Principles in

the Use of Animals in Toxicology outlined by Society of Toxicology and the European Union Directive 2010/63/EU for animal experiments, and received approval from the Peking University Institutional Review Board.

The TiO_2 NPs were dispersed in ultrapure water and sonicated for 15 min. In order to obtain a homogenized suspension, the particle suspension was vortexed before every use. Suspensions of TiO_2 NPs (0, 2, 10, 50 mg per kg BW) were administered to rats *via* oral gavage in a volume of 1 mL daily for 30 consecutive days. The intragastric doses of TiO_2 NPs for rats were selected based on the oral intake of TiO_2NPs for children under the age of 10 years in the US.[6]

The symptoms and mortality were observed and recorded daily throughout the entire duration of exposure up to 30 days. The body weight of rats was assessed every 7 days and the food intake of rats was recorded every 3–4 days. During the experiments, no significant changes in the body weight and food intake of the exposed rats were found (ESI, Fig. S1 and S2†) and no mortality was observed. After 7, 14 and 28 days, rat feces were collected and quickly transferred and stored at −80 °C in a refrigerator. Then after 30 days, animals were weighed and sacrificed. The blood samples were collected from the abdominal aorta. Serum was harvested by centrifuging blood at 3000 rpm (1500*g*) for 10 min. The colon tissues were harvested and partially homogenized.

2.3 Histopathological analysis

For pathological studies, all histopathological examinations were performed using standard laboratory procedures. The colon tissues were embedded in paraffin blocks, then sliced into 5 μm in thickness and placed onto glass slides. After hematoxylin–eosin (HE) staining, the slides were observed and photos were taken using an optical microscope (OlympusBX50, Moticam 2306, Japan). The pathologist who performed the observation and analysis was blinded of the treatment group and dosing regimen.

2.4 Transmission electron microscopy (TEM) observation

For TEM observation, the tissues of colon were cut up into small pieces (1 mm^3) and immediately fixed in 2.5% glutaraldehyde (pH 7.4) overnight. Then the colon samples were treated according to the general protocols for the TEM study. The ultra-thin sections (70–100 nm) were stained with lead citrate and uranyl acetate. The specimens were examined using a JEOL JEM-1400 electron microscope.

2.5 16S rDNA sequencing and gut microbiota analysis

Genomic DNA of fecal samples was extracted by the Cetyltrimethylammonium Ammonium Bromide (CTAB) method after water was removed by using freeze-drying apparatus. After the purity and concentration of DNA were detected by agarose gel electrophoresis, DNA samples were diluted with sterile water to 1 ng μL^{-1}. PCR amplification was conducted by using the diluted genomic DNA as the template, and the specific primers with Barcode, Phusion® High-Fidelity PCR Master Mix with GC Buffer and high-efficiency fidelity enzyme. The PCR amplification system was as follows: 2× taq PCR mix: 25 μl; Primer F (10 μM): 1 μl; Primer FR (10 μM): 1 μl; gDNA: 2.5 μl; H_2O: 8.0 μl. The procedure of PCR amplification was as follows: (1) 95 °C for 5 min; (2) step a–c cycle 34 times, (a) 94 °C for 1 min, (b) 57 °C for 45 s, (c) 72 °C for 1 min; (3) 72 °C for 10 min; (4) 16 °C for 5 min. The primer sequence was as follows (5′–3′): V4-515F, GTGCCAGCMGCCGCGGTAA; V4-806R, GGACTACHVGGGTWTCTAAT; V3 + V4-341F, CCTAYGGGRBGCASCAG; V3 + V4-806R, GGACTAC-NNGGGTATCTAAT; V4 + V5-515F, GTGCCAGCMGCCGCGGTAA; V4 + V5-907R, CCGTCAAT-TCCTTTGAGTTT. The V3–V5 region of 16S rRNA gene extracted from fecal specimens was amplified by universal primers. The PCR product was detected by electrophoresis with 2% agarose gel. According to the concentration of the PCR product, the sample was mixed equally. After mixing fully, the PCR product was purified by 2% agarose gel electrophoresis with 1× TAE, and the target band was cut and recycled. A GeneJET gel recovery kit was used to recover the purified product. Sequencing libraries were generated using an Ion Plus Fragment Library Kit 48 rxns library kit. The libraries were quantified by Qubit fluorescence and then single-End sequencing was performed by using an Ion S5™XL sequencer. Small fragment libraries were constructed for sequencing. The operation steps in the experiment were strictly in accordance with the instructions.

QIIME (Version 1.9.1) software was used to filter the mosaic data. Subsequently, the sequence data obtained are compared with the sequence in 16S: gold database, and the chimera sequence is detected and removed to obtain an effective sequence (clean reads) for subsequent analysis. Uparse (v7.0.1001) software was used to cluster all clean reads and sequences with similarity greater than 97% were clustered into an Operational Taxonomic Unit (OTU). The pseudo-OTUs caused by chimeras were discriminated and filtered. The OTUs of each sample were obtained, and the sequence with the highest frequency of each OTU was selected as the representative sequence. The Mothur algorithm and SILVA SSU r132 database were used to annotate the representative sequences of OTUs and obtain taxonomic information. The community compositions of each sample were counted at levels of kingdom, phylum, class, order, family, genus and species. Using MUSCLE (Version 3.8.31) software for fast multi-sequence alignment, the phylogenetic relationships of all OTUs representative sequences were obtained. Finally, according to the sequence with the least amount of data in the sample, the data of each sample were normalized. The normalized data were used in the subsequent Alpha and Beta diversity analysis to compare the different bacteria community structure among different experimental groups. KRONA was used to visualize the results of species annotation. The first 10 species with the highest abundance in each taxonomic hierarchy (phylum, class, order, family, genus, species) were selected to draw a cylindrical accumulative map of relative abundance of species generated by a taxonomic tree. LEfSe (Linear Discriminant Analysis Effect Size) software was used to compare the species differences among groups. Linear

Discriminant Analysis (LDA) was used to find the different intestinal bacteria among groups (LDA Score >4).

2.6 Measurement of lipopolysaccharides (LPS) and short-chain fatty acids (SCFAs)

The LPS content in the feces was measured using ELISA kits (Wuhan Abebio Science Co., Ltd, China) according to the manufacturer's instructions. The assay employed a two-site sandwich ELISA to quantitate LPS in samples. SCFAs in the feces, including acetic acid (AA), propionic acid (PA), isobutyric acid (IBA), butyric acid (BA), isovaleric acid (IVA), and hexanoic acid (HA), were assayed by targeted metabolomics using GC-MS/MS (Thermo, USA). Samples were weighed 100 mg in a 2 ml EP tube and mixed with 1 mL phosphoric acid (0.5% v/v) solution for 10 minutes. 0.02 mL solution above was added to a 1.5 mL centrifugal tube, and 1 mL MTBE (containing the internal standard) solution was added, then the resulting solution was subjected to ultrasonication in an ice bath for 5 minutes. The solution was centrifuged for 10 minutes at 12 000 rpm and 4 °C. Then 0.5 mL of the supernatant and 0.5 mL MTBE were absorbed into the injection bottle, waiting for GC-MS/MS analysis. Key parameters for GC-MS/MS analysis are shown in Table S3.† The software Agilent Mass Hunter was used for data processing. Quality control samples (QC) were prepared by mixing sample extracts to monitor the repeatability of the analysis process.

2.7 Metabolomic analysis

The method for feces metabolomic analysis refers to the protocol of Want *et al.*[39]

Homogenate of feces tissue and sample preparation. 30.0 mg vacuum-dried feces were added to 900 μl pre-cooled methanol/water (1 : 1) solution. Then it was homogenized at 30 000 rpm on ice for 30 s (homogenized for 10 seconds, cooled for 30 seconds, repeated three times) and blended by vortexing for 20 seconds and stored at −20 °C overnight. And then, the homogenate was centrifuged (16 000*g*, 4 C) for 10 minutes and the supernatant was taken. The supernatant was dried and concentrated in a low temperature vacuum concentrator and for 4 hours. Re-suspension was carried out by using 200 μl methanol/water (1 : 1) solvent before analysis. Meanwhile, 20 μl of each sample was taken and then divided into three parts after gentle mixing as quality control (QC) samples, which were prepared for technical repetition to evaluate the stability and repeatability of the experimental instruments and methods.

Non-targeted metabolomics analysis using HPLC-MS. An Ultra High Performance Liquid Chromatography-Q-Exactive Orbitrap-High-resolution Mass Spectrometry System (UPLC-QEMS, U3000, Thermo, USA) was used for non-targeted metabolomics analysis. The samples were randomly injected after disruption of the order to control the possible impact of instrumental stability fluctuation. Three QC samples were analyzed before experimental samples, after half of all samples and after all samples, respectively. The QEMS was equipped with an electrospray ionization source (ESI). Fragmentation was achieved by high-energy collision dissociation (HCD). The normalized collision energies were 15, 30 and 45 eV, respectively. The results were measured by positive ion mode and negative ion mode. The mass scanning range was 50–1100 m/z, and the total scanning resolution of parent ions (MS) was 60 K.

Analysis and annotation of mass spectrometry data. The original result file obtained by instrument analysis (.raw format file, positive and negative ion mode data) is imported into Compound Discoverer 3.0 software (Thermo Fisher Scientific, USA) for peak alignment, deconvolution, noise filtering, mass-charge correction and baseline correction. The parameters are set as follows: retention time (RT) < 0.2 min; signal-to-noise ratio (SNR) > 3; the DDA mode was used to analyze secondary ion mass spectra (MS_2); signal intensity >500 000 included in the analysis; the filling gap algorithm was used to extract and fill the peaks (more parameters for metabolite identification by Compound Discoverer software are shown in Table S1†).

The annotation and identification of metabolites were carried out through a software-related mzCloud database and mzVault database. The peak area was used as the relative concentration for subsequent analysis. The data containing the metabolite identification results and peak area were pretreated. The relative concentration of metabolites was completely clustered using the Euclidean distance, and the Heatmap was drawn to show the difference of the concentrations of metabolites in each sample. Principal Component Analysis (PCA) was used to reduce the dimension of the original data and observe the difference trend and potential outlier value of samples. Using the orthogonal projection to latent structure discriminant analysis (OPLS-DA) model to screen biomarkers that change after TiO_2 NP exposure, the OPLS-DA model score maps were drawn by the first predictive component (T score [1]) and the first orthogonal component (Orthogonal T score [1]). Through Simica-P. software (V14.1, Umetrics, Sweden), the permutation test of the OPLS-DA model is performed to verify the stability of the OPLS-DA model. Then the V-plot was drawn according to the covariance (p1) and reliability (p(corr)1) of the first principal component of each variable in the OPLS-DA model, and the metabolite with an absolute value of p(corr)1 greater than 0.3 in the V-plot is selected as the differential metabolite.

After obtaining the differential metabolites, the KEGG metabolic pathway was analyzed by the Pathway Analysis function module in Metaboanalyst 4.0 website. The significantly changed pathway was determined by false discovery rate (FDR) < 0.05, and pathway impact greater than 0.10.

2.8 Detection of oxidative stress biomarkers and inflammatory cytokines

Oxidative damage to the colon following repeated TiO_2 NP exposure was evaluated by the presence of glutathione, glutathione peroxidase (GSH-Px), lipid peroxidation products (malondialdehyde, MDA), superoxide dismutase (SOD), and sulfhydryl groups (SH) in tissue homogenates. The levels of gluta-

thione, including reduced (GSH) and oxidized (GSSG) glutathione, were tested using commercial kits (Nanjing Jiancheng Bioengineering Institute, Jiangsu, China). GSH-Px, MDA, SOD and SH were measured in colon homogenates using the Colorimetric Assay Kits (Beijing Leagene Biotechnology Inc, Beijing, China). Inflammatory cytokines in serum from rats exposed to TiO_2 NPs repeatedly were analyzed by tumor necrosis factor a (TNF α) and interleukin 6 (IL-6), using an enzyme-linked immuno sorbent assay (ELISA) kit (Abcam, USA).

2.9 Statistical analysis

Methods of statistical analysis for data of feces metabolomics and gut microbiota were described above. Other data were expressed as means ± SD and analyzed with SPSS 20.0. One-way variance (ANOVA) with LSD or Dunnet'T3 tests was applied to evaluate the statistical significance of differences between the experimental groups and the controls. A p value of less than 0.05 was considered to be statistically significant.

3. Results

3.1 Physicochemical properties of TiO_2 nanoparticles

The majority of the TiO_2 NPs used in this study were spherical and anatase crystals with a purity of 99.90%. As shown in Fig. 1, the average size of the TiO_2 NPs measured by SEM was 29 ± 9 nm. The EDX combined with SEM confirmed that the atomic ratio of Ti and O was 1 : 2. The measured Brunauer–Emmett–Teller (BET) specific surface area of the TiO_2 NPs was 77.51 $m^2\ g^{-1}$. In order to characterize TiO_2 NPs in the exposure medium and rat gastrointestinal tract, the hydrodynamic diameter and zeta potential of TiO_2 NPs (1 mg mL^{-1}) in ultrapure water (H_2O), artificial gastric juice (AGJ) and artificial intestinal juice (AIJ) were tested. As shown in Fig. 1, it was clear that the hydrodynamic size of TiO_2 NPs was bigger in H_2O, AGJ and AIJ than their primary size, which was likely due to the aggregation and the adsorption of biomolecules. Furthermore, a change from positive to negative of zeta potential was also observed in the exposure medium of AIJ. And the zeta potential of NPs in all three solutions was around ±10 mV, which may be due to the acidity or basicity of these fluids. These results suggested that TiO_2 NPs tended to agglomerate to form larger particles in the gastrointestinal tract.

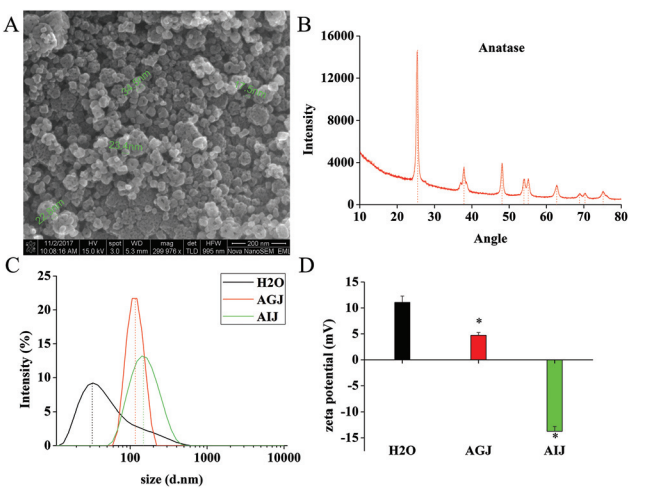

Fig. 1 Characterization of TiO_2 NPs. (A) The representative SEM image of TiO_2 NPs. (B) The crystal analysis chart for TiO_2 NPs by XRD. The hydrodynamic diameter (C) and zeta potential (D) of TiO_2 NPs (1 mg mL^{-1}) in ultrapure water (H_2O), artificial gastric juice (AGJ) and artificial intestinal juice (AIJ). Significant difference compared with the group of TiO_2 NPs in H_2O (*p < 0.05).

3.2 Effects of TiO_2 nanoparticles on colon morphology of rats after oral exposure for 30 days

Fig. 2 shows the changes of colon morphology of rats induced by oral exposure to TiO_2 nanoparticles for 30 days. The representative pathological and transmission electron micrographs of the colon tissue sections were presented. HE staining pathological images showed that the number of goblet cells in colon epithelium decreased and inflammatory cells infiltrated in the

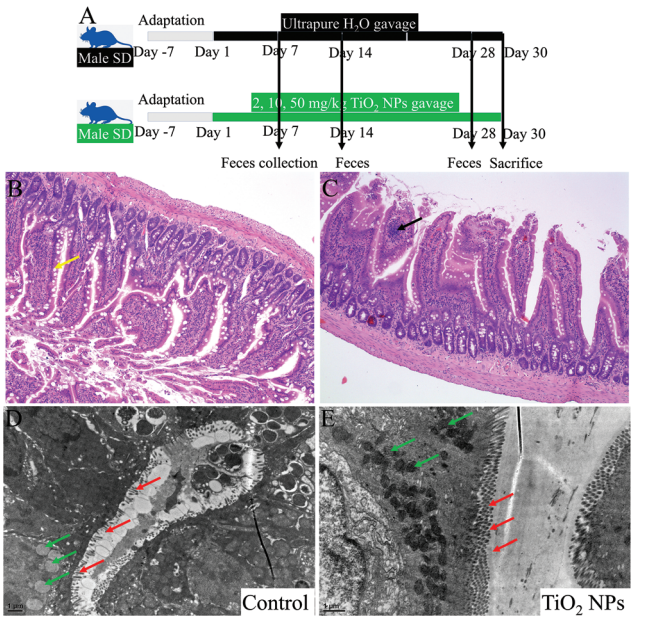

Fig. 2 Effects of TiO_2 nanoparticles on colon morphology of rats after oral exposure for 30 days. (A) Schematic diagram for oral administration of TiO_2 NPs (0, 2, 10 and 50 mg per kg per day) in SD rats for 30 days. The colon morphology was evaluated by histopathological and transmission electron microscopy (TEM) observation. (B) and (C) are representative pathological images of HE staining under light microscopy (magnification: 200×). HE staining pathological images showed that the number of goblet cells decreased and inflammatory cells infiltrated in colon epithelium in the 50 mg per kg BW TiO_2 NP treated rats. (D) and (E) are representative TEM images of colon tissues (magnification: 8000×). Under TEM, it was observed that pyknosis and dissolution of crista in most mitochondria (green arrows) of colonic epithelia were obvious in the 50 mg per kg BW TiO_2 NP treated group. However, the number of microvilli (red arrow) of colonic epithelia in the TiO_2 NP treated group increased significantly.

50 mg per kg BW TiO_2 NP treated rats. Meanwhile, transmission electron microscopy (TEM) was used to observe the colonic ultrastructure of rats after oral exposure to TiO_2 NPs. TEM images revealed that pyknosis and dissolution of crista in most mitochondria occurred in the high dose exposure group. However, the number of microvilli of colonic epithelia in the exposure group increased significantly. These results indicated that oral exposure to TiO_2 NPs induced a certain degree of colon injury in rats.

3.3 Effects of TiO_2 nanoparticles on gut microbiota

The structure and composition of gut microbiota communities at phylum, class, order, family, genus and species levels (top ten) are shown in Fig. 3. Top two relative abundances of bacteria at the phylum-level were *Bacteroidetes* and *Firmicutes*, which accounted for more than 95% of the total. Top two relative abundances of bacteria at the class-level were *Bacterodia* and *Clostridia*, which accounted for more than 66% of the total. Consistently, the top two relative abundances of bacteria at the order-level were *Bacteroidales* and *Clostridiates.* At family, genus and species-levels, the classification of bacteria tended to be dispersed. There was no significant change in the total observed species (Fig. 4A). The comparison of alpha (α) diversity and beta (β) diversity of gut microbiota between groups is also shown in Fig. 4. The indexes of Shannon, Simpson, Chao1, ACE and PD_Whole_Tree were used for the comparison of alpha (α) diversity of gut microbiota, none of which changed significantly. The same result was obtained by

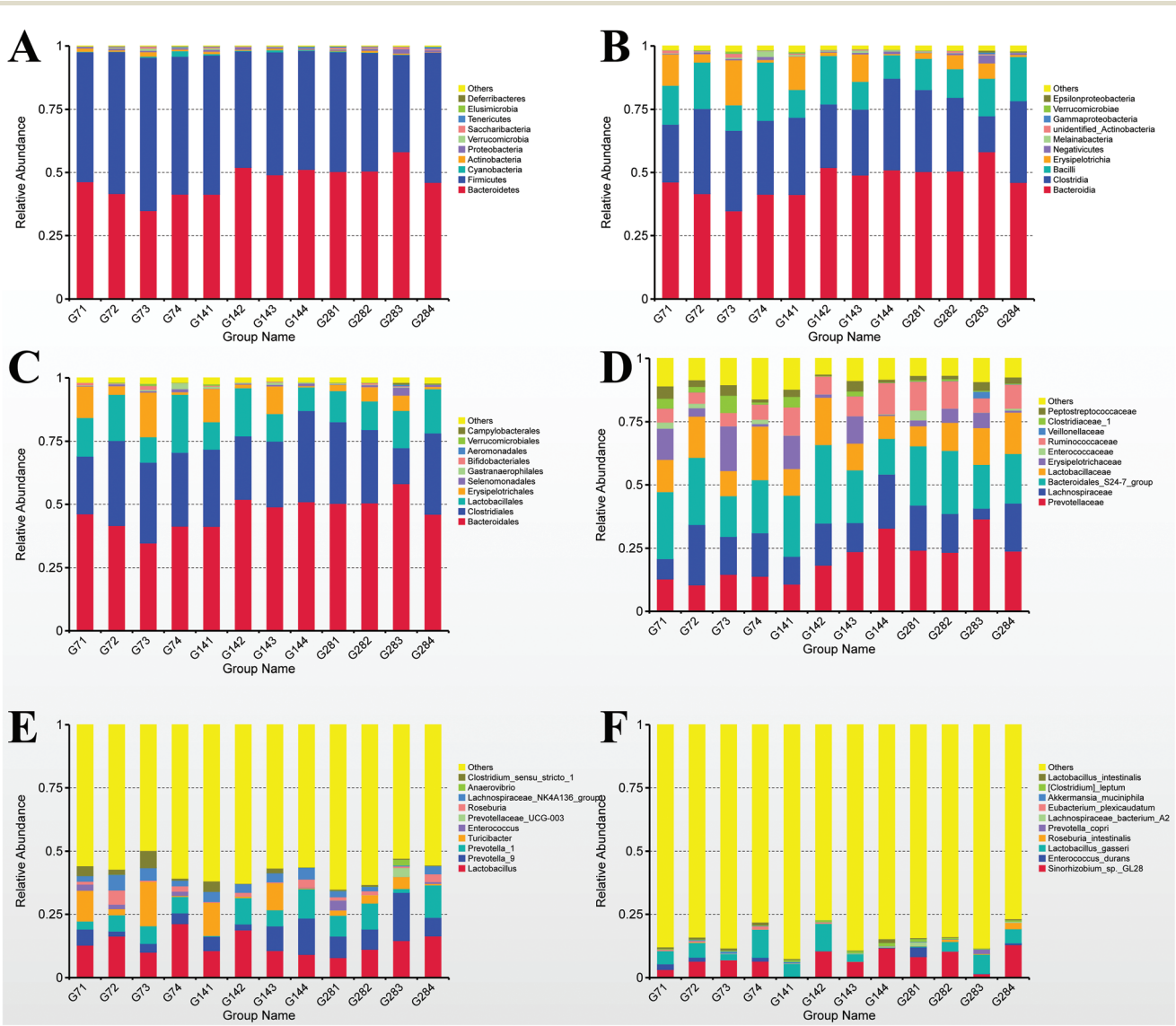

Fig. 3 Effect of TiO_2 nanoparticles on gut microbiota after oral administration for 7, 14 and 28 days. Top ten relative abundances of bacteria at the phylum (A), class (B), order (C), family (D), genus (E), and species (F) levels. G71, G141, G281: control group (0 mg per kg BW TiO_2 NPs) for 7, 14 and 28 days, respectively; G72, G142, G282: low-dose exposure group (2 mg per kg BW TiO_2 NPs) for 7, 14 and 28 days, respectively; G73, G143, G283: medium-dose exposure group (10 mg per kg BW TiO_2 NPs) for 7, 14 and 28 days, respectively; G74, G144, G284: high-dose exposure group (50 mg per kg BW TiO_2 NPs) for 7, 14 and 28 days, respectively.

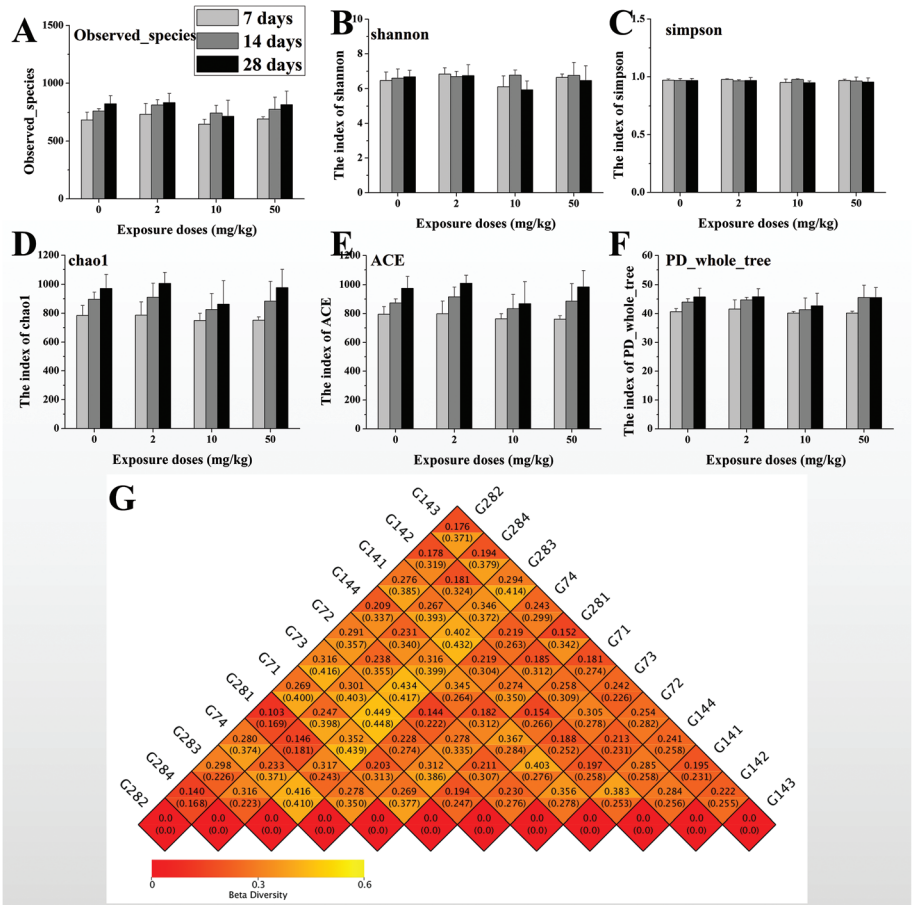

Fig. 4 Comparison of observed species and diversity of gut microbiota between different groups. The observed species were compared between different groups (A). The indexes of Shannon (B), Simpson (C), Chao1 (D), ACE (E) and PD_Whole_Tree (F) were used for the comparison of alpha (α) diversity of gut microbiota. (G) Comparison of beta (β) diversity of gut microbiota between different groups. G71, G141, G281: control group (0 mg per kg BW TiO_2 NPs) for 7, 14 and 28 days, respectively; G72, G142, G282: low-dose exposure group (2 mg per kg BW TiO_2 NPs) for 7, 14 and 28 days, respectively; G73, G143, G283: medium-dose exposure group (10 mg per kg BW TiO_2 NPs) for 7, 14 and 28 days, respectively; G74, G144, G284: high-dose exposure group (50 mg per kg BW TiO_2 NPs) for 7, 14 and 28 days, respectively.

comparison of beta (β) diversity of gut microbiota between different groups. However, LefSe analysis identified some differentially expressed strains among different groups (Fig. 5). After oral exposure to TiO_2 NPs for 7 days, no significant changes were observed in the flora. By the 14th day, 3 differentially expressed strains (LDA Score >4) were obtained, all of which belong to *Firmicutes*. They were *Bacteria.Firmicutes.Bacilli.Lactobacillales.Lactobacillaceae.Lactobacillus.Lactobacillus_gasseri* (*L. gasseri*), *Bacteria.Firmicutes.Erysipelotrichia.Erysipelotrichales.Erysipelotrichaceae.Turicibacter* (*Turicibacter*) and *Bacteria.Firmicutes.Negativicutes.Selenomonadales.Veillonellaceae.Veillonella* (*Veillonella*). *L. gasseri* increased significantly in the high-dose group. *Turicibacter* increased significantly in the low-dose group. *Veillonella* decreased significantly in the exposure groups. By the 28th day, 2 differentially expressed strains (LDA Score >4) were obtained. They were *Bacteria.Firmicutes.Bacilli.Lactobacillales.Lactobacillaceae.Lactobacillus.Lactobacillus_gasseri* (*L. gasseri*) and *Bacteria.Firmicutes.Clostridia.Clostridiales.Lachnospiraceae.Lachnospiraceae_NK4A136_group* (*L. NK4A136_group*). *L. gasseri* increased significantly in the high-dose group, consistent with the results of the 14th day. The *L. NK4A136_group* increased significantly in the medium-dose group.

3.4 Effect of TiO_2 nanoparticles on gut-associated metabolism

As shown in Fig. 6A, the heatmap showed that there were differences in the expression of some metabolites among different groups. PCA results showed that there was a clear separation trend between the TiO_2 NP exposure group and the control group, suggesting that there was a significant change in metabolites between different groups (Fig. 6B). The score map of the OPLS-DA model effectively distinguishing the samples of different groups further validated the above results (Fig. 6C).

As shown in Fig. 7A, 25 metabolites differentially expressed between groups were screened, using the V-plot of the OPLS-DA model and p(corr)1 > 0.3 as the criterion. Among them, the concentrations of 9 metabolites including

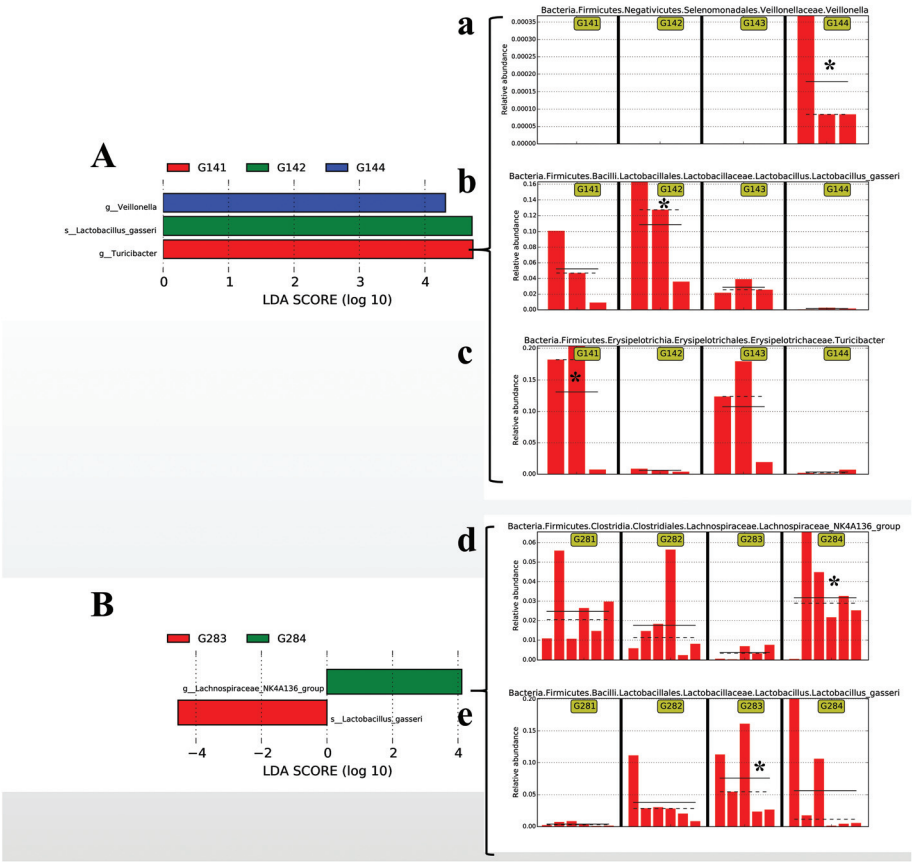

Fig. 5 Differentially expressed strains of gut microbiota between the samples in different groups. (A) Bacteria with enrichment (LDA > 4) in the control group and low and high dose groups exposed to TiO_2 NPs for 14 days. *L. gasseri* (a) increased significantly in the high-dose group. *Turicibacter* (b) increased significantly in the low-dose group. *Veillonella* (c) decreased significantly in the exposure groups. (B) Bacteria with enrichment (LDA > 4) in the medium and high dose groups exposed to TiO_2 NPs for 28 days. *L. gasseri* increased significantly in the high-dose group, consistent with the results of the 14th day. The *L. NK4A136_group* increased significantly in the medium-dose group. * represents the statistical difference ($p < 0.05$). G141, G281: control group (0 mg per kg BW TiO_2 NPs) for 14 and 28 days, respectively; G142, G282: low-dose exposure group (2 mg per kg BW TiO_2 NPs) for 14 and 28 days, respectively; G143, G283: medium-dose exposure group (10 mg per kg BW TiO_2 NPs) for 14 and 28 days, respectively; G144, G284: high-dose exposure group (50 mg per kg BW TiO_2 NPs) for 14 and 28 days, respectively.

N-acetylhistamine, caprolactam, glycerophosphocholine, pyridoxine, 2,3,5,6-tetramethylpyrazine, tryptamine, cytosine, adenosine, and D-pipecolinic acid increased significantly compared with the control group. And 16 metabolites including 4-methyl-5-thiazoleethanol, L-histidine, L-ornithine, *etc.* decreased significantly (detailed information of differential metabolites is shown in Table S2†).

Most of the differential metabolites belonged to the super class of organic acids and derivatives (12 metabolites) and organoheterocyclic compounds (10 metabolites). Among the increased metabolites induced by TiO_2 NPs, organoheterocyclic compounds, containing a ring with least one carbon atom and one non-carbon atom, accounted for the largest proportion (5/9). Among the decreased metabolites induced by TiO_2 NPs, organic acids and derivatives accounted for the largest proportion (10/16). Compared with the control group, metabolites with the greatest changes of the relative concentration in the TiO_2 NP exposure group were *N*-acetylhistamine (9.29-fold increase), caprolactam (9.06-fold increase), glycerophosphocholine (8.16-fold increase), 4-methyl-5-thiazoleethanol (9.69-fold decrease), L-histidine (9.57-fold decrease), and L-ornithine (8.60-fold decrease).

Pathway topology analysis found that the aminoacyl-tRNA biosynthesis metabolic pathway (FDR = 0.046, pathway impact = 0.103) significantly changed in the TiO_2 NP exposure group (Fig. 7B).

3.5 Changes of lipopolysaccharides (LPS) and short-chain fatty acids (SCFAs)

As shown in Fig. 8A, LPS content in the serum increased significantly in the TiO_2 NP exposure groups compared with the control group. LPS are a major component of the outer membrane of Gram-negative bacteria, whose death results if it is mutated or removed. The increase of LPS content should be the result of the changes of gut microbiota. SCFAs, known as volatile fatty acids, play important roles in the metabolism of different organs in the human body. The type and quantity of SCFAs mainly depend on the compo-

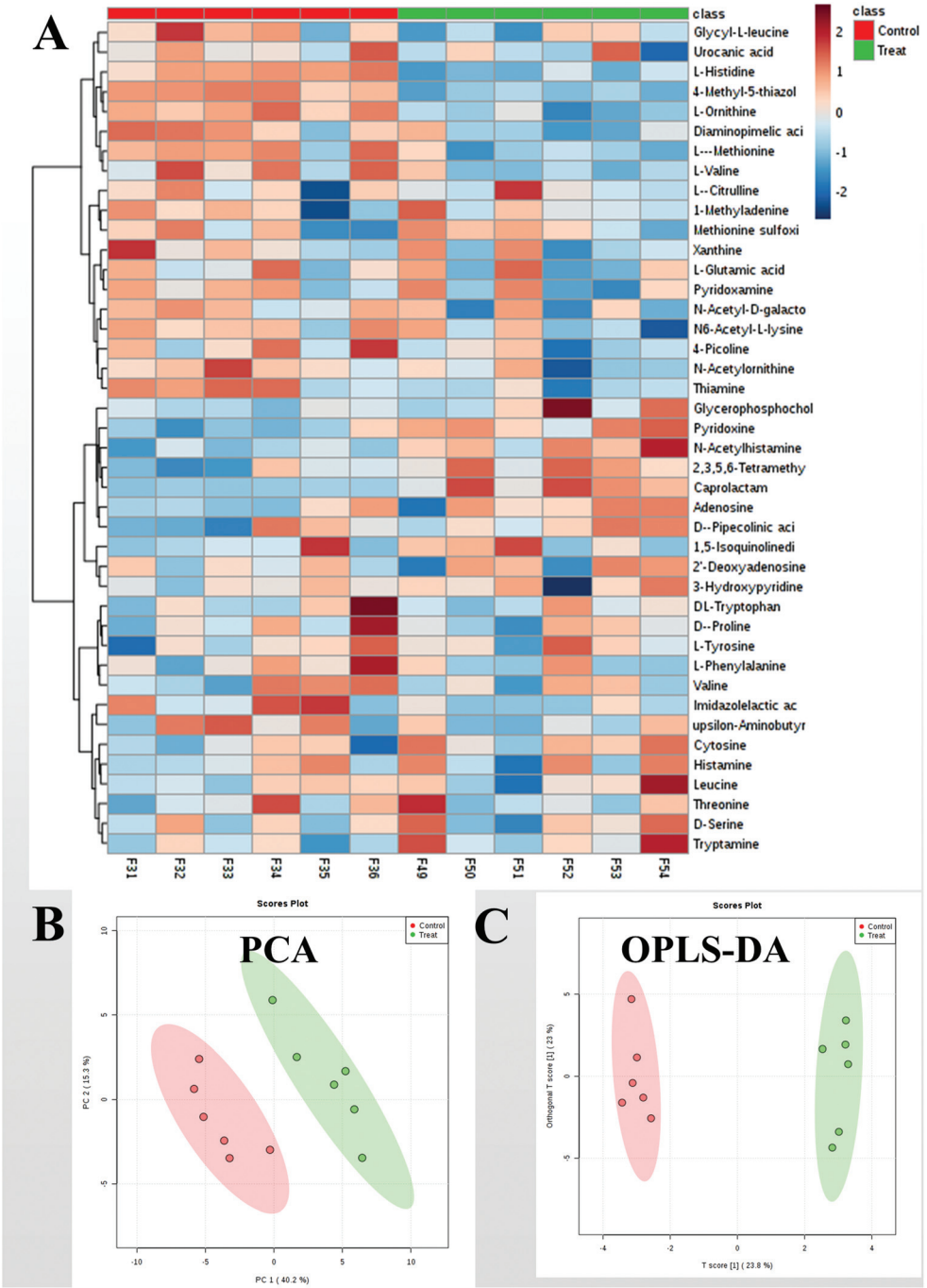

Fig. 6 Effect of TiO_2 nanoparticles on gut-associated metabolism analyzed by non-targeted metabolomics in feces using HPLC-MS. (A) Heatmap of metabolite concentrations, which shows the different metabolites in feces of rats in the control group and high-dose TiO_2 NP (50 mg kg^{-1}) treated group for 30 days. Each row represents a metabolite, and each column represents a sample. The color of each grid represents the relative concentration of the metabolites in the corresponding sample. (B) PCA and (C) OPLS-DA scoring maps of metabolites in the control and TiO_2 NP treated group samples.

sition of gut microbiota, digestion time and host microbial generation. We found that six SCFAs in the feces, including acetic acid (AA), propionic acid (PA), isobutyric acid (IBA), butyric acid (BA), isovaleric acid (IVA) and hexanoic acid (HA), did not change significantly after exposure to TiO_2 NPs (Fig. 8B).

3.6 Oxidative stress and inflammatory response

Several markers of oxidative stress, including the levels of reduced (GSH) and oxidized (GSSG) glutathione, MDA, and sulfhydryl groups (SH) and the activity of GSH-Px and SOD, were measured in colon tissues of rats after oral exposure to

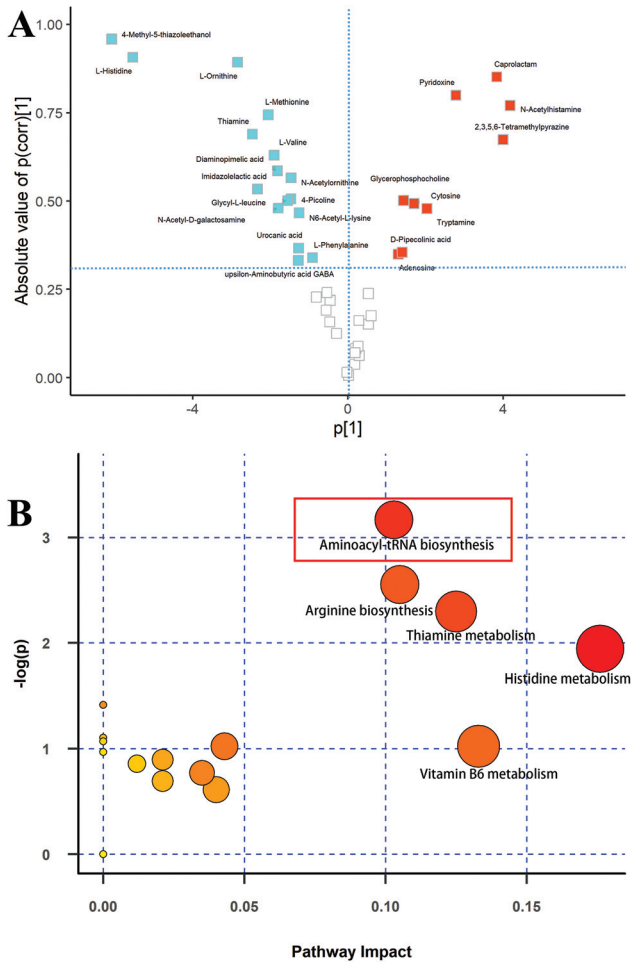

Fig. 7 Differential metabolites and metabolic pathway between the feces samples in the control and TiO_2 NP (50 mg kg^{-1}) treated group. (A) V Score Map of metabolites using the OPLS-DA model. *X*-Axis represents the difference between groups and *Y*-axis represents the reliability of differences between groups. Taking p(corr) > 0.3 as the demarcation value, the red points with name annotations indicated that the concentrations of the metabolites in the TiO_2 NP (50 mg kg^{-1}) treated group were higher than those in the control group. The blue points with name annotations indicated that the concentrations of the metabolites in the TiO_2 NP (50 mg kg^{-1}) treated group were lower than those in the control group. (B) KEGG pathway analysis of differential metabolites between the samples in the control and TiO_2 NP (50 mg kg^{-1}) treated group. *X*-Axis represents the Pathway Impact obtained by the out-degree centrality algorithm. The size of the point is related to the Pathway Impact. *Y*-Axis represents the negative logarithm of the *p* value (−log(*p*)) obtained by the pathway enrichment analysis. The yellow-red color change of the point is positively related to the −log(*p*). The names of pathways are labeled in the graph with −log(*p*) > 1 or pathway impact > 0.1. The aminoacyl-tRNA biosynthesis metabolic pathway highlighted by a red box was significantly enriched in the TiO_2 NP (50 mg kg^{-1}) treated group.

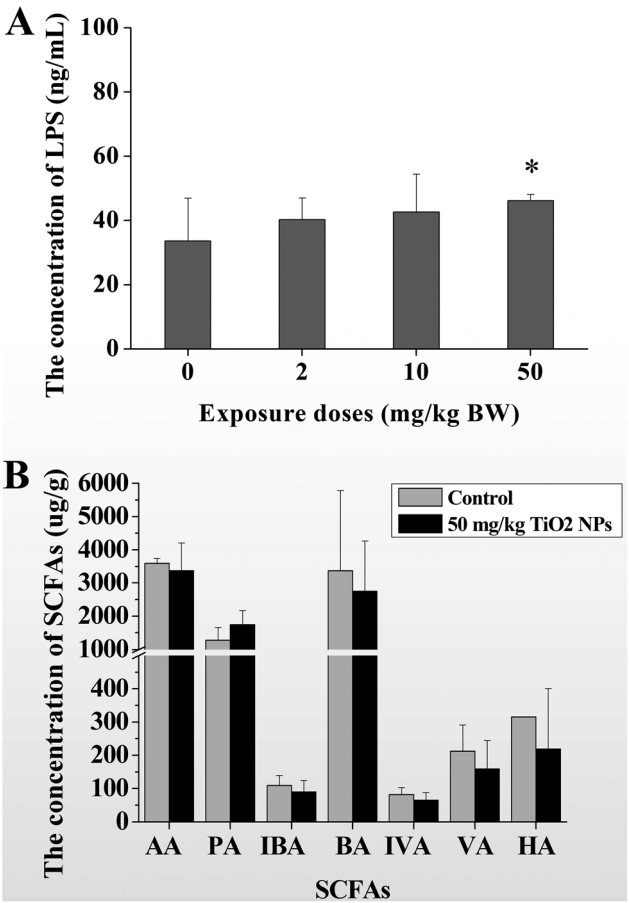

Fig. 8 Effect of TiO_2 NPs on the content of LPS in the serum and SCFAs in the feces. (A) LPS content increased significantly in the TiO_2 NP exposure groups compared with the control group. (B) SCFAs, including acetic acid (AA), propionic acid (PA), isobutyric acid (IBA), butyric acid (BA), isovaleric acid (IVA) and hexanoic acid (HA), did not change significantly after exposure to TiO_2 NPs. Significant difference compared to the control group (*p < 0.05). LPS: lipopolysaccharides; SCFAs: short-chain fatty acids.

TiO_2 NPs for 30 days (Table 1). The increased content of MDA and decreased activity of SOD were found in rats after TiO_2 NP exposure compared to those in the control group. TiO_2 NPs caused accumulation of lipid peroxidation (MDA) and decreased activity of antioxidant enzyme (SOD), indicating that the redox balance was destroyed. Meanwhile, we evaluated the inflammatory status of rats by quantifying the concentrations of inflammatory cytokines in serum. We observed increased concentration of IL-6 in the serum of rats treated with 50 mg kg^{-1} TiO_2 NPs for 30 days. The changes of oxidative stress biomarkers and inflammatory cytokines suggested that the oxidative stress state and inflammatory response were induced by oral exposure of TiO_2 NPs.

4. Discussion

In the present study, we focused on the effects of TiO_2 NPs on gut microbiota and gut-associated metabolism in rats, exploring the potential role of gut microbiota imbalance in toxicity induced by oral administration of TiO_2 NPs. Generally, TiO_2 NPs may induce toxicity through direct and indirect pathways. The direct pathway refers to the accumulation of TiO_2 NPs in

Table 1 Effect of TiO_2 NPs on oxidative stress biomarkers and inflammatory cytokines in serum of rats after oral exposure for 30 days

		TiO_2 NP treated doses (mg per kg BW)		
	Control	2	10	50
GSH (μmol mg^{-1} protein)	13.38 ± 6.4	13.28 ± 6.84	15.82 ± 1.3	14.32 ± 3.27
GSSG (μg mg^{-1} protein)	13.5 ± 6.96	18.79 ± 8.88	19.11 ± 4.12	16.61 ± 4.85
GSH-Px (mU mg^{-1} protein)	17.38 ± 16.06	21.21 ± 10.91	18.28 ± 5.52	14.62 ± 8.64
MDA (nmol mg^{-1} protein)	41.73 ± 7.35	50.98 ± 6.47*	44.21 ± 6.04	54.55 ± 8.76*
SOD (U mg^{-1} protein)	2.49 ± 0.54	2.64 ± 0.51	2.15 ± 0.31*	2.29 ± 0.2
SH (nmol mg^{-1} protein)	33.12 ± 11.23	26.49 ± 15.02	12.29 ± 11.14	29.89 ± 16.56
IL-6 (pg mL^{-1})	22.87 ± 17.74	29.84 ± 19.89	39.57 ± 10.24	31.28 ± 5.94*
TNF-α (pg mL^{-1})	42.25 ± 25.27	54.92 ± 32.1	48.92 ± 14.54	38.49 ± 11.29

*Significant difference compared to the control group ($p < 0.05$). NPs, nanoparticles; BW, body weight; GSH, reduced glutathione; GSH-Px, glutathione peroxidase; GSSG, oxidized glutathione; MDA, malondialdehyde, lipid peroxidation products; SOD, superoxide dismutase; SH, sulfhydryl group; IL, interleukin; TNF, tumor necrosis factor.

the organs after absorption by the digestive tract, thereby impairing the tissues directly. Previous toxicokinetics studies showed that the oral absorption of TiO_2 NPs was very low and most of them were excreted with feces.[15] A small amount may be transported and distributed to the liver, spleen, kidneys, lungs and brain under high-dose (such as 5000 mg per kg body weight) oral exposure.[40,41] Studies have demonstrated that orally ingested TiO_2 NPs can induce significant impact on the liver,[40,42,43] kidney,[44] heart,[40] haemostasis blood system[43] immune response[43] and reproductive system.[45] The ability of TiO_2 NPs to generate excessive free radicals and ROS was considered to be the main reason for tissue damage.[46] The redox imbalance could induce inflammation and mitochondrial dysfunction, leading to cellular apoptosis or death.[47,48] However, when no obvious deposition was found in the organs, understanding the mechanism of toxic effects became a noticeable issue.[15,42] Cho *et al.*[15] used lower doses (520.8, 1041.5 and 2083 mg per kg BW) and longer exposure time for 13 weeks, but found that the content of Ti elements was not significantly changed in the liver, spleen, kidneys, and brain of SD rats. Our previous study also found that the contents of titanium in the blood, liver, kidneys and spleen of rats in the TiO_2 NP-treated groups were not significantly different from those in the control group after oral exposure to 200 mg kg^{-1} TiO_2 NPs for 30 days.[42] This indicated that the toxicokinetics of TiO_2 NPs after longer exposure time at lower doses may be quite different from that after short-term and high-dose exposure. But the liver and kidneys were still found to be slightly damaged after long-term and low-dose exposure.[42] Since TiO_2 NPs were not deposited in these organs, we didn't think it caused toxicity of target tissues through the direct pathway. As most of the orally ingested TiO_2 NPs were excreted through feces,[15] the interaction between TiO_2 NPs and gut microbiota was suspected to be an important indirect pathway.

Originally, TiO_2 NPs were reported to be a unique antimicrobial compound due to their excellent photocatalytic activity. The oxygen free radicals and ROS produced by TiO_2 NPs in the presence of ultraviolet or visible light could disrupt bacterial cell walls and cause cell death.[32,33] Recent studies found that even in the absence of light, TiO_2 NPs also had a significant antimicrobial effect on intestinal bacteria such as *E. coli.*[34,35] And the TiO_2 NPs with a smaller particle size produced a higher content of intracellular ROS, in line with their greater antibacterial effect.[31] In view of the fact that most of the orally ingested TiO_2 NPs were not absorbed and mainly acted in the digestive tract as well as its antimicrobial activity, it is reasonable to believe that it would affect gut microbiota. In the present study, we confirmed that orally ingested TiO_2 NPs affected gut microbiota of rats, monitoring and analyzing by 16S rDNA sequencing. Rat feces were collected after oral exposure for 7, 14 and 28 days. The structure and composition of gut microbiota communities changed over time. At the same time point, we found differentially expressed bacterial strains among different exposure groups until the 14th day. By the 14th day, 3 differentially expressed strains were obtained, including *L. gasseri*, *Turicibacter* and *Veillonella*. By the 28th day, 2 differentially expressed strains were obtained, including *L. gasseri* and the *L. NK4A136_group*. All of these differentially expressed strains belong to *Firmicutes* at the phylum-level. The results were supported by some previous *in vitro* studies. Waller *et al.*[36] used the model colon reactor *in vitro* exposure to TiO_2 NPs (25 nm) for 5 consecutive days and found that TiO_2 NPs could rapidly remodel the composition of intestinal bacteria *in vitro*, and change the relative abundance of intestinal bacteria such as *Firmicutes*.

TiO_2 NPs induced the increase of *L. gasseri* both after 14 and 28 days of exposure (Fig. 5), indicating that it may be a key intestinal flora affected by orally ingested TiO_2 NPs. *L. gasseri* is a kind of *Bacteria.Firmicutes.Bacilli.Lactobacillales.Lactobacillaceae.Lactobacillus.Lactobacillus_gasseri* (classification) and an anaerobic, Gram-positive bacterium that falls into the category of lactic acid bacteria. It is typically found in the gastrointestinal tracts of humans and animals due to its largely fermentative function. *L. gasseri* participates in fermentative actions which produce lactic acid as well as the energy required for growth. However, it was also reported that this bacterium could make hydrogen peroxide (H_2O_2)[49] and was identified as a cause of Fournier's gangrene.[50] *L. gasseri* also played a part in regulating the immune function in humans, which decreased the levels of the IgE in perennial allergic rhi-

nitis patients.[51] An experimental study demonstrated that *L. gasseri* producing manganese SOD had significant anti-inflammatory activity reducing the severity of colitis in IL-10-deficient mice.[52] The increase of *L. gasseri* in the present study may be an adaptive response to the oxidative stress state and inflammation induced by oral exposure of TiO_2 NPs.

The other differentially expressed strains induced by TiO_2 NPs were also biologically related. *Turicibacter* is a genus in the *Firmicutes* phylum of bacteria that has most commonly been found in the guts of animals.[53] It was reported that *Turicibacter* may be important for the abnormal metabolism of type 2 diabetes mellitus (T2DM).[54] This was similar to the effect of another differential bacterium *L. NK4A136_group.* Cui *et al.*[55] found that the abundance of the *L. NK4A136_group* of gut microbiota was significantly associated with the therapeutic effects of purified anthraquinone-glycoside preparation from rhubarb (RAGP) on the T2DM. In addition, the *L. NK4A136_group* has been reported to be related to dysbiosis of the gut microbiota induced by environmental factors, such as lead and polyene phosphatidylcholine (PPC).[56,57] *Veillonella* are Gram-negative anaerobic cocci and belongs to the family *Veillonellaceae*. *Veillonella* are part of the normal flora of the mouth and gastrointestinal tract and may be found in the vagina as well. Of limited pathogenicity, *Veillonella* species are common and considered mainly harmless.[58] Decreased abundance of *Veillonella* may be the result of the imbalance of gut microbiota community.

Changes in the structure and abundance of gut microbiota may affect their metabolic function. Modifications to the gut microbiota can provide signals through the intestine and bacterial products that affect metabolism at different levels. So, metabolomics analysis of feces was conducted to further explore the gut-associated metabolic changes. We observed the significant disturbance of metabolites in feces of rats orally exposed to TiO_2 NPs. Bioinformatics analysis of fecal metabolomics showed that there was an obvious distinction in the metabolic spectrum between the TiO_2 NP exposure group and the control group. 25 metabolites differentially expressed between groups were screened. Changes in metabolites may cause various biological effects, which in turn affected the health of the host. *N*-Acetylhistamine that was differentially expressed in the exposure group is 4-(beta-acetylaminoethyl) imidazole that is generated from histamine *via* the enzyme transferase. It is an intermediate in histidine metabolism. Interestingly, a significant change in the L-histidine level was also observed, which further demonstrated that histidine metabolism may be disordered. L-Histidine is an alpha-amino acid with an imidazole functional group. It is one of the 22 proteinogenic amino acids. L-Histidine is a precursor for histamine and carnosine biosynthesis. L-Histidine and other imidazole compounds have anti-oxidant, anti-inflammatory and anti-secretory properties.[59,60] The efficacy of L-histidine in protecting inflamed tissue is attributed to the capacity of the imidazole ring to scavenge reactive oxygen species (ROS).[59] In the present study, the oxidative stress state and inflammatory response were induced by oral exposure of TiO_2 NPs. The decrease of L-histidine may be related to this biological effect, but the causal relationship was not clear. Moreover, L-histidine may have many other possible functions because it is the precursor of the ubiquitous neurohormone–neurotransmitter histamine. The metabolic disorders of histidine and histamine may be related to the reported neurotoxicity induced by TiO_2 NPs.[61,62]

Glycerophosphorylcholine (GPC) is a choline derivative and one of the two major forms of choline storage (along with phosphocholine) in the cytosol. The increase of GPC we observed in the TiO_2 NP exposure group may be due to elevated choline levels leading to increased cell storage. The elevated choline may be one of the causes of lipid metabolism disorder we found earlier.[63] Choline can synthesize phosphatidylcholine and assemble into very low density lipoproteins to transport triglycerides from the liver to other tissues.[64] In addition, differentially expressed metabolites including L-ornithine and L-histidine indicated the interference of TiO_2 NPs on amino acid metabolism. L-Ornithine is produced in the urea cycle through the cleavage of urea from arginine. Mitochondrial abnormalities of colonic epithelia in the high dose TiO_2 NP exposure group were revealed by TEM observation. And, mitochondrial dysfunction may result in disorders of the L-ornithine metabolism and urea cycle.[65] It is well known that mitochondria are closely related to energy metabolism. Mitochondria containing a variety of redox enzymes during tricarboxylic acid (TCA) cycle are the key subcellular organelle of energy metabolism. Previous *in vitro* and *in vivo* studies have shown that the energy-related metabolic pathway could be affected by the exposure of TiO_2 NPs.[66,67] Chen *et al.*[66] reported that TiO_2 NPs increased ROS of mitochondria and decreased ATP production in macrophage cells (RAW). In addition, Ratnasekhar *et al.*[67] showed that TiO_2 NPs could cause significant changes in the TCA cycle metabolic pathway of *Caenorhabditis elegans*. Indeed, our previous study had found that TiO_2 NPs could induce an increased level of hepatic glucose metabolism.[68] Mitochondrial damage induced by TiO_2 NPs may be the cause of energy metabolism disorder.

Variations in metabolites have led to our interest in the major metabolic pathways that TiO_2 NPs affected. Bioinformatics analysis showed that the aminoacyl-tRNA biosynthesis metabolic pathway was significantly enriched by integrating differentially expressed metabolites. Aminoacyl-tRNAs (aa-tRNAs) are the essential substrates for translation. The aminoacyl-tRNA biosynthesis pathway map involves the metabolism of many amino acids,[69] such as L-histidine. Complex formation between enzymes in the same pathway may protect the fidelity of protein synthesis. The aminoacyl-tRNA biosynthesis pathway belongs to the classification of genetic information processing and may mainly affect the translation process of gut microbiota.

In addition, we found oxidative stress in colon tissues and inflammatory responses in serum of rats after oral administration of TiO_2 NPs for 30 days (Table 1). Previous studies had demonstrated that oxidative stress and inflammatory responses were indirect pathways for toxicity induced by oral

exposure to the TiO_2 NPs. Trouiller *et al.*[70] suggested that the genotoxicity *in vivo* in mice induced by oral intake of TiO_2 NPs (100 mg per kg BW for 5 days) may be mainly associated with the inflammation and/or oxidative stress, which was called a secondary genotoxic mechanism. Afterwards, several publications confirmed that the genotoxicity of most nanomaterials (NMs) is likely to be associated with indirect consequences of inflammation and generation of oxidative species by inflammatory cells (neutrophils and macrophages).[71–74] However, the original sites of oxidative stress and inflammation induced by TiO_2 NPs and their more advanced mechanism, such as how to cause them, remain unclear. In the present study, we found the increased content of lipopolysaccharides (LPS) in serum of rats exposed to TiO_2 NPs, which should be the result of the changes of gut microbiota. LPS-induced ROS and inflammatory responses had been widely reported.[75] LPS have been implicated as a potent inducer of inflammatory responses, along with the release of ROS from mitochondria.[76,77] Elevated levels of ROS are responsible for producing various biological events, such as peroxidation of lipids and proteins as well as oxidative damage of DNA. Therefore, we considered that oxidative stress and inflammation induced by TiO_2 NPs may be originally related to the increase of LPS, which was primarily due to gut microbiota disorders.

According to our results, the alteration of gut microbiota and gut-associated metabolism may be the primary mechanism for toxicity induced by oral administration of TiO_2 NPs, which is summarized and shown in Fig. 9. The changes of gut microbiota were represented by increased *L. gasseri*, *Turicibacter*, and *L. NK4A136_group* and decreased *Veillonella*, leading to the changes of gut-associated metabolism. The increased metabolites were represented by *N*-acetylhistamine, caprolactam, and glycerophosphocholine, and the increased metabolites were represented by 4-methyl-5-thiazoleethanol, L-histidine, and L-ornithine in the TiO_2 NP exposure group. The aminoacyl-tRNA biosynthesis metabolic pathway significantly changed. Metabolic disorders of gut microbiota and subsequently produced LPS led to oxidative stress and an inflammatory response in the intestine, which was considered to be a key and primary indirect pathway for toxicity induced by oral exposure to TiO_2 NPs. This mechanism may be suitable for most cases of toxicity caused by oral intake of nanomaterials. Because nanomaterials generally have higher surface activity, they can easily interact with gut microbiota and generally possess potential antimicrobial activity.[78] We provided a new scientific clue for exploring the mechanisms of biological effects of nanomaterials after dietary and environmental exposure.

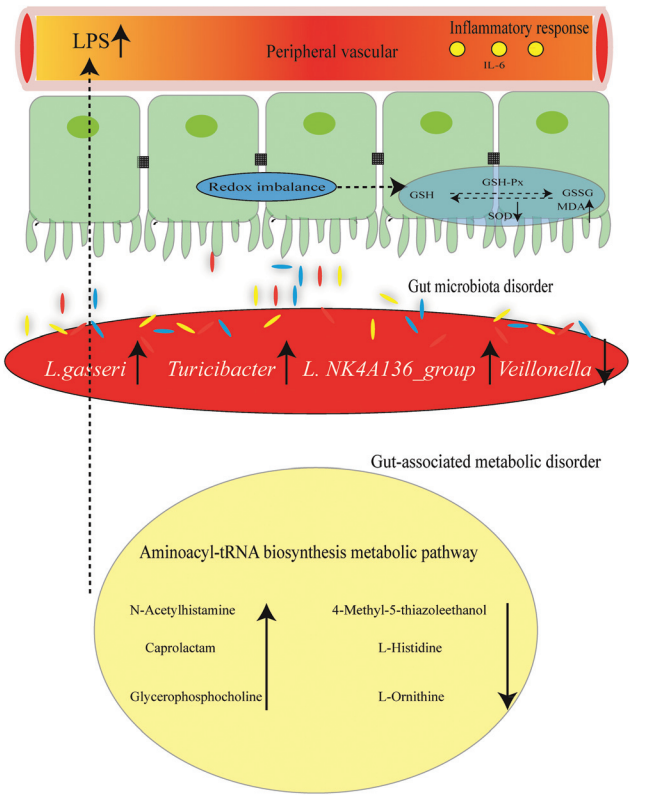

Fig. 9 Interaction of gut microbiota, gut-associated metabolism and toxicity induced by oral exposure to TiO_2 NPs. The alteration of gut microbiota and gut-associated metabolism may be the primary mechanism for toxicity induced by oral administration of TiO_2 NPs. The changes of gut microbiota represented by increased *L. gasseri*, *Turicibacter*, and *L. NK4A136_group* and decreased *Veillonella* led to the changes of gut-associated metabolism. The increased metabolites represented by *N*-acetylhistamine, caprolactam, glycerophosphocholine, and the increased metabolites represented by 4-methyl-5-thiazoleethanol, L-histidine, and L-ornithine in the TiO_2 NP exposure group. The aminoacyl-tRNA biosynthesis metabolic pathway significantly changed. Metabolic disorders of gut microbiota and subsequently produced LPS led to oxidative stress and inflammatory response in the intestine, which was considered to be a key and primary indirect pathway for toxicity induced by oral exposure to the TiO_2 NPs.

5. Conclusions

In conclusion, orally ingested TiO_2 NPs could induce disorders of gut microbiota and gut-associated metabolism. The indirect pathway of oxidative stress and inflammatory response, probably due to stimulation of LPS produced by gut microbiota primarily, played an important role in the underlying mechanisms of toxicity induced by oral exposure to TiO_2 NPs. This may be a common mechanism for toxicity caused by oral intake of most nanomaterials. Attention should be paid to the health risk of dietary and environmental exposure to nanoparticles.

Conflicts of interest

No potential conflict of interest was reported by the authors.

Acknowledgements

This work was supported by the National Natural Science Foundation of China (81703257) and the National Key R&D Program of the Ministry of Science and Technology of China (2017YFC1600204).

References

1 S. H. Othman, N. R. Abd Salam, N. Zainal, R. K. Basha and R. A. Talib, *Int. J. Photoenergy*, 2014, 945930.
2 V. J. Morris, *Trends Biotechnol.*, 2011, **29**, 509–516.
3 I. S. Sohal, K. S. O'Fallon, P. Gaines, P. Demokritou and D. Bello, *Part. Fibre Toxicol.*, 2018, **15**, DOI: 10.1186/s12989-018-0265-1.
4 X. Chen and S. S. Mao, *Chem. Rev.*, 2007, **107**, 2891–2959.
5 Y. Yang, K. Doudrick, X. Bi, K. Hristovski, P. Herckes, P. Westerhoff and R. Kaegi, *Environ. Sci. Technol.*, 2014, **48**, 6391–6400.
6 A. Weir, P. Westerhoff, L. Fabricius, K. Hristovski and N. von Goetz, *Environ. Sci. Technol.*, 2012, **46**, 2242–2250.
7 X.-X. Chen, B. Cheng, Y.-X. Yang, A. Cao, J.-H. Liu, L.-J. Du, Y. Liu, Y. Zhao and H. Wang, *Small*, 2013, **9**, 1765–1774.
8 C. Rompelberg, M. B. Heringa, G. van Donkersgoed, J. Drijvers, A. Roos, S. Westenbrink, R. Peters, G. van Bemmel, W. Brand and A. G. Oomen, *Nanotoxicology*, 2016, **10**, 1404–1414.
9 C. S. U. Demirel, N. C. Birben and M. Bekbolet, *Chemosphere*, 2018, **211**, 420–448.
10 M. Pelaez, N. T. Nolan, S. C. Pillai, M. K. Seery, P. Falaras, A. G. Kontos, P. S. M. Dunlop, J. W. J. Hamilton, J. A. Byrne, K. O'Shea, M. H. Entezari and D. D. Dionysiou, *Appl. Catal., B*, 2012, **125**, 331–349.
11 A. J. Wyrwoll, P. Lautenschlaeger, A. Bach, B. Hellack, A. Dybowska, T. A. J. Kuhlbusch, H. Hollert, A. Schaeffer and H. M. Maes, *Environ. Pollut.*, 2016, **208**, 859–867.
12 M. B. Heringa, R. J. B. Peters, R. L. A. W. Bleys, M. K. van der Lee, P. C. Tromp, P. C. E. van Kesteren, J. C. H. van Eijkeren, A. K. Undas, A. G. Oomen and H. Bouwmeester, *Part. Fibre Toxicol.*, 2018, **15**, DOI: 10.1186/s12989-018-0251-7.
13 H. Shi, R. Magaye, V. Castranova and J. Zhao, *Part. Fibre Toxicol.*, 2013, **10**, DOI: 10.1186/1743-8977-10-15.
14 M. Shakeel, F. Jabeen, S. Shabbir, M. S. Asghar, M. S. Khan and A. S. Chaudhry, *Biol. Trace Elem. Res.*, 2016, **172**, 1–36.
15 W.-S. Cho, B.-C. Kang, J. K. Lee, J. Jeong, J.-H. Che and S. H. Seok, *Part. Fibre Toxicol.*, 2013, **10**, DOI: 10.1186/1743-8977-10-9.
16 K. Jones, J. Morton, I. Smith, K. Jurkschat, A.-H. Harding and G. Evans, *Toxicol. Lett.*, 2015, **233**, 95–101.
17 F. Aguilar, R. Crebelli, A. Di Domenico, B. Dusemund, M. J. Frutos, P. Galtier, D. Gott, U. Gundert-Remy, C. Lambre, J.-C. Leblanc, O. Lindtner, P. Moldeus, A. Mortensen, P. Mosesso, D. Parent-Massin, A. Oskarsson, I. Stankovic, I. Waalkens-Berendsen, R. A. Woutersen, M. Wright and M. Younes, *EFSA J.*, 2016, **14**, DOI: 10.2903/j.efsa.2016.4545.
18 L. Geraets, A. G. Oomen, P. Krystek, N. R. Jacobsen, H. Wallin, M. Laurentie, H. W. Verharen, E. F. A. Brandon and W. H. de Jong, *Part. Fibre Toxicol.*, 2014, **11**, DOI: 10.1186/1743-8977-11-30.
19 J. M. Kinross, A. W. Darzi and J. K. Nicholson, *Genome Med.*, 2011, **3**, DOI: 10.1186/gm228.
20 E. Holmes, J. V. Li, T. Athanasiou, H. Ashrafian and J. K. Nicholson, *Trends Microbiol.*, 2011, **19**, 349–359.
21 A. Biragyn and L. Ferrucci, *Lancet Oncol.*, 2018, **19**, E295–E304.
22 A. B. Hall, A. C. Tolonen and R. J. Xavier, *Nat. Rev. Genet.*, 2017, **18**, 690–699.
23 K. Honda and D. R. Littman, *Nature*, 2016, **535**, 75–84.
24 Y. Jin, S. Wu, Z. Zeng and Z. Fu, *Environ. Pollut.*, 2017, **222**, 1–9.
25 S. M. Dizaj, F. Lotfipour, M. Barzegar-Jalali, M. H. Zarrintan and K. Adibkia, *Mater. Sci. Eng., C*, 2014, **44**, 278–284.
26 A. Besinis, T. De Peralta and R. D. Handy, *Nanotoxicology*, 2014, **8**, 1–16.
27 J. T. Seil and T. J. Webster, *Int. J. Nanomed.*, 2012, **7**, 2767–2781.
28 A. Khezerlou, M. Alizadeh-Sani, M. Azizi-Lalabadi and A. Ehsani, *Microb. Pathog.*, 2018, **123**, 505–526.
29 L. Brunet, D. Y. Lyon, E. M. Hotze, P. J. J. Alvarez and M. R. Wiesner, *Environ. Sci. Technol.*, 2009, **43**, 4355–4360.
30 S. Sharifi, S. Behzadi, S. Laurent, M. L. Forrest, P. Stroeve and M. Mahmoudi, *Chem. Soc. Rev.*, 2012, **41**, 2323–2343.
31 X. Lin, J. Li, S. Ma, G. Liu, K. Yang, M. Tong and D. Lin, *PLoS One*, 2014, **9**, DOI: 10.1371/journal.pone.0110247.
32 F. Chen, X. Yang, F. Xu, Q. Wu and Y. Zhang, *Environ. Sci. Technol.*, 2009, **43**, 1180–1184.
33 K. Page, M. Wilson and I. P. Parkin, *J. Mater. Chem.*, 2009, **19**, 3819–3831.
34 B. Sohm, F. Immel, P. Bauda and C. Pagnout, *Proteomics*, 2015, **15**, 98–113.
35 H. Kong, J. Song and J. Jang, *Environ. Sci. Technol.*, 2010, **44**, 5672–5676.
36 T. Waller, C. Chen and S. L. Walker, *Environ. Eng. Sci.*, 2017, **34**, 537–550.
37 A. A. Taylor, I. M. Marcus, R. L. Guysi and S. L. Walker, *Environ. Eng. Sci.*, 2015, **32**, 602–612.
38 A. Pietroiusti, A. Magrini and L. Campagnolo, *Toxicol. Appl. Pharmacol.*, 2016, **299**, 90–95.
39 E. J. Want, P. Masson, F. Michopoulos, I. D. Wilson, G. Theodoridis, R. S. Plumb, J. Shockcor, N. Loftus, E. Holmes and J. K. Nicholson, *Nat. Protoc.*, 2013, **8**, 17–32.
40 J. Wang, G. Zhou, C. Chen, H. Yu, T. Wang, Y. Ma, G. Jia, Y. Gao, B. Li, J. Sun, Y. Li, F. Jiao, Y. Zhao and Z. Chai, *Toxicol. Lett.*, 2007, **168**, 176–185.
41 R. Zhang, Y. Niu, Y. Li, C. Zhao, B. Song, Y. Li and Y. Zhou, *Environ. Toxicol. Pharmacol.*, 2010, **30**, 52–60.
42 Y. Wang, Z. Chen, T. Ba, J. Pu, T. Chen, Y. Song, Y. Gu, Q. Qian, Y. Xu, K. Xiang, H. Wang and G. Jia, *Small*, 2013, **9**, 1742–1752.
43 Y. Duan, J. Liu, L. Ma, N. Li, H. Liu, J. Wang, L. Zheng, C. Liu, X. Wang, X. Zhao, J. Yan, S. Wang, H. Wang, X. Zhang and F. Hong, *Biomaterials*, 2010, **31**, 894–899.
44 S. Gui, Z. Zhang, L. Zheng, Y. Cui, X. Liu, N. Li, X. Sang, Q. Sun, G. Gao, Z. Cheng, J. Cheng, L. Wang, M. Tang and F. Hong, *J. Hazard. Mater.*, 2011, **195**, 365–370.

45 X. Zhao, Y. Ze, G. Gao, X. Sang, B. Li, S. Gui, L. Sheng, Q. Sun, J. Cheng, Z. Cheng, R. Hu, L. Wang and F. Hong, *PLoS One*, 2013, **8**, DOI: 10.1371/journal.pone.0059378.
46 R. K. Shukla, A. Kumar, N. V. S. Vallabani, A. K. Pandey and A. Dhawan, *Nanomedicine*, 2014, **9**, 1423–1434.
47 R. K. Shukla, A. Kumar, D. Gurbani, A. K. Pandey, S. Singh and A. Dhawan, *Nanotoxicology*, 2013, **7**, 48–60.
48 R. K. Shukla, V. Sharma, A. K. Pandey, S. Singh, S. Sultana and A. Dhawan, *Toxicol. in Vitro*, 2011, **25**, 231–241.
49 M. C. Otero and M. E. Nader-Macias, *Anim. Reprod. Sci.*, 2006, **96**, 35–46.
50 I. M. Tleyjeh, J. Routh, M. O. Qutub, G. Lischer, K. V. Liang and L. M. Baddour, *Scand. J. Infect. Dis.*, 2004, **36**, 501–503.
51 H. Morita, F. He, M. Kawase, A. Kubota, M. Hiramatsu, J.-I. Kurisaki and S. Salminen, *Microbiol. Immunol.*, 2006, **50**, 701–706.
52 I. M. Carroll, J. M. Andrus, J. M. Bruno-Barcena, T. R. Klaenhammer, H. M. Hassan and D. S. Threadgill, *Am. J. Physiol.: Gastrointest. Liver Physiol.*, 2007, **293**, G729–G738.
53 T. A. Auchtung, M. E. Holder, J. R. Gesell, N. J. Ajami, R. T. D. Duarte, K. Itoh, R. R. Caspi, J. F. Petrosino, R. Horai and C. R. Zarate-Blades, *Microbiol. Resour. Announc.*, 2016, **4**, DOI: 10.1128/genomeA.00114-16.
54 M. Horie, T. Miura, S. Hirakata, A. Hosoyama, S. Sugino, A. Umeno, K. Murotomi, Y. Yoshida and T. Koike, *Exp. Anim.*, 2017, **66**, 405–416.
55 H.-X. Cui, L.-S. Zhang, Y. Luo, K. Yuan, Z.-Y. Huang and Y. Guo, *Front. Microbiol.*, 2019, **10**, DOI: 10.3389/fmicb.2019.01423.
56 D. Cheng, H. Li, J. Zhou and S. Wang, *Food Funct.*, 2019, **10**, 681–690.
57 H. Yu, Z. Yu, H. Huang, P. Li, Q. Tang, X. Wang and S. Shen, *BioFactors*, 2019, **45**, 439–449.
58 J. Washio, Y. Shimada, M. Yamada, R. Sakamaki and N. Takahashi, *Appl. Environ. Microbiol.*, 2014, **80**, 4184–4188.
59 J. W. Peterson, I. Boldogh, V. L. Popov, S. S. Saini and A. K. Chopra, *Lab. Invest.*, 1998, **78**, 523–534.
60 U. H. Ramadhan and N. J. Al-Salihi, *E-J. Chem.*, 2011, **8**, 1832–1842.
61 R. Hu, X. Gong, Y. Duan, N. Li, Y. Che, Y. Cui, M. Zhou, C. Liu, H. Wang and F. Hong, *Biomaterials*, 2010, **31**, 8043–8050.
62 A. Mohammadipour, M. Hosseini, A. Fazel, H. Haghir, H. Rafatpanah, M. Pourganji and A. E. Bideskan, *Toxicol. Ind. Health*, 2016, **32**, 221–228.
63 Z. Chen, Y. Wang, L. Zhuo, S. Chen, L. Zhao, X. Luan, H. Wang and G. Jia, *Toxicol. Lett.*, 2015, **239**, 123–130.
64 Z. Li and D. E. Vance, *J. Lipid Res.*, 2008, **49**, 1187–1194.
65 H. Morizono, J. E. Woolston, M. Colombini and M. Tuchman, *Mol. Genet. Metab.*, 2005, **86**, 431–440.
66 Q. Chen, N. Wang, M. Zhu, J. Lu, H. Zhong, X. Xue, S. Guo, M. Li, X. Wei, Y. Tao and H. Yin, *Redox Biol.*, 2018, **15**, 266–276.
67 C. Ratnasekhar, M. Sonane, A. Satish and M. K. R. Mudiam, *Nanotoxicology*, 2015, **9**, 994–1004.
68 Z. Chen, Y. Wang, X. Wang, L. Zhuo, S. Chen, S. Tang, L. Zhao, X. Luan and G. Jia, *J. Appl. Toxicol.*, 2018, **38**, 810–823.
69 C. Polycarpo, A. Ambrogelly, A. Berube, S. A. M. Winbush, J. A. McCloskey, P. F. Crain, J. L. Wood and D. Soll, *Proc. Natl. Acad. Sci. U. S. A.*, 2004, **101**, 12450–12454.
70 B. Trouiller, R. Reliene, A. Westbrook, P. Solaimani and R. H. Schiestl, *Cancer Res.*, 2009, **69**, 8784–8789.
71 N. Golbamaki, B. Rasulev, A. Cassano, R. L. M. Robinson, E. Benfenati, J. Leszczynski and M. T. D. Cronin, *Nanoscale*, 2015, **7**, 2154–2198.
72 N. R. Jacobsen, P. Moller, K. A. Jensen, U. Vogel, O. Ladefoged, S. Loft and H. Wallin, *Part. Fibre Toxicol.*, 2009, **6**, DOI: 10.1186/1743-8977-6-2.
73 Z. Magdolenova, A. Collins, A. Kumar, A. Dhawan, V. Stone and M. Dusinska, *Nanotoxicology*, 2014, **8**, 233–278.
74 M. V. D. Z. Park, A. M. Neigh, J. P. Vermeulen, L. J. J. de la Fonteyne, H. W. Verharen, J. J. Briede, H. van Loveren and W. H. de Jong, *Biomaterials*, 2011, **32**, 9810–9817.
75 R. Wiest, M. Lawson and M. Geuking, *J. Hepatol.*, 2014, **60**, 197–209.
76 M. S. Khan, T. Ali, M. W. Kim, M. H. Jo, M. G. Jo, H. Badshah and M. O. Kim, *Neurochem. Int.*, 2016, **100**, 1–10.
77 L. Qin, X. Wu, M. L. Block, Y. Liu, G. R. Breese, J.-S. Hong, D. J. Knapp and F. T. Crews, *Glia*, 2007, **55**, 453–462.
78 S. J. Lam, E. H. H. Wong, C. Boyer and G. G. Qiao, *Prog. Polym. Sci.*, 2018, **76**, 40–64.